


2D Repetitive PI Control for Enhanced Harmonic Current Suppression in Induction Machines

Johannes Stoß 


Elektrotechnisches Institut (ETI)
Karlsruhe Institute of Technology
Karlsruhe, Germany
johannes.stoss@kit.edu

Pierre Mader

Elektrotechnisches Institut (ETI)
Karlsruhe Institute of Technology
Karlsruhe, Germany

Stephan Goehner 

Elektrotechnisches Institut (ETI)
Karlsruhe Institute of Technology
Karlsruhe, Germany
stephan.goehner@kit.edu

Leonard Geier 


Elektrotechnisches Institut (ETI)
Karlsruhe Institute of Technology
Karlsruhe, Germany
leonard.geier@kit.edu

Matthias Brodatzki

Elektrotechnisches Institut (ETI)
Karlsruhe Institute of Technology
Karlsruhe, Germany
matthias.brodatzki@kit.edu

Marc Hiller

Elektrotechnisches Institut (ETI)
Karlsruhe Institute of Technology
Karlsruhe, Germany
marc.hiller@kit.edu

Andreas Liske 

Elektrotechnisches Institut (ETI)
Karlsruhe Institute of Technology
Karlsruhe, Germany
andreas.liske@kit.edu

Abstract— This paper presents a novel control strategy, for mitigating harmonics in squirrel cage induction machines using a repetitive PI-controller. The proposed method enhances existing control architectures for permanent-magnet synchronous motors by taking the rotor harmonics into account by adding a second dimension. This is a key enabler for harmonic current mitigation in induction machines, as the magnetic circuit depends on the rotor position and rotor flux angle. The presented controller has been verified by test bench measurements. In addition, its performance is demonstrated by comparison with a conventional PI control and a 1D repetitive PI control using measurements.

Keywords— induction machines, harmonics, non-linear control, harmonics mitigation, machine control

I. INTRODUCTION

The operation of electric machines inherently generates current harmonics, which affect both system efficiency and performance [1], [2], [3]. The primary sources of current harmonics are the machine design [4], [5], [6] and the power inverter nonlinearities [7], [8]. Various control strategies are known to reduce the current harmonics in induction machine drive systems. In [9], the harmonic content is reduced by incorporating morphological filters within the feedback loop, which minimizes the superimposed harmonics caused by the PI-control itself. [10] introduces a quasi-resonant linear active disturbance rejection based current loop control method for harmonic mitigation. [11] suggests using different PI-control loops in rotating reference frames to additionally reduce the 5th and 7th harmonic components in doubly fed induction machines. In [12] a resonant controller is proposed in to specifically target and reduce the 5th and 7th harmonics in the stator current.

In this paper a novel approach is presented, which extends existing control methods for PMSMs [7], [13] to comply with the harmonic content of induction machines. Due to the design as repetitive controller, mitigation as well as precise injection of current harmonics are possible [7]. In contrast to existing methods, the repetitive control algorithm can therefore reduce a wide range of harmonic components.

This work starts by deriving the origin of harmonic current components in squirrel cage induction machines, motivating the need for a two-dimensional control approach. This is followed by a brief description of the control design and parameterization. Verification is done through testbench measurements, demonstrating the performance of the novel control design by comparison to existing methods

II. CURRENT HARMONICS IN INDUCTION MACHINES

As mentioned in the introduction, the primary sources of current harmonics are inverter nonlinearities and the machine itself. Since the harmonics generated by the inverter are similar across various types of machines, this chapter focuses on the induction machine as the cause of current harmonics.

The analysis is based on the electro magnetic machine model of the induction motor. Using the voltage equations of the induction machine, the relationship between the flux linkages and current harmonics can be explained. Since the control is based on rotor flux orientation (RFO), the modeling also utilizes the rotor flux-oriented dq coordinate system.

The dq stator voltages (v_{sd} , v_{sq}) are expressed as functions of the stator resistance R_S , the stator dq currents (i_{sd} , i_{sq}), stator flux linkages (ψ_{sd} , ψ_{sq}) and the stator angular velocity ω_S .

$$v_{sd} = R_S \cdot i_{sd} + \frac{d\psi_{sd}}{dt} - \psi_{sq} \cdot \omega_S \quad (1)$$

$$v_{sq} = R_S \cdot i_{sq} + \frac{d\psi_{sq}}{dt} + \psi_{sd} \cdot \omega_S \quad (2)$$

The rotor voltage equations are similarly defined using the corresponding rotor quantities. Since the rotor is short-circuited, its voltages are $v_{Rd} = v_{Rq} = 0$.

Due to the rotor flux orientation, ψ_{Rq} is zero by definition and is consequently excluded from the equations.

$$v_{Rd} = 0 = R_R \cdot i_{Rd} + \frac{d\psi_{Rd}}{dt} \quad (3)$$

$$v_{Rq} = 0 = R_R \cdot i_{Rq} + \psi_{Rd} \cdot \omega_R \quad (4)$$

In stationary operation, the voltages v_{sd} and v_{sq} show only little variation. As a result, current harmonics are mainly formed due to the flux linkages. Elimination is therefore only possible if the output voltages of the inverter are chosen as a function of the flux linkages. For this purpose, angular dependencies of the flux linkages are examined using FEA data of an example machine generated with the method presented in [4].

A. Spatial harmonics of flux linkage maps

As the machine design differs from the device under test (DUT) shown in chapter IV, only the basic principle is explained based on the data. Direct application to the test bench or controller parameterization cannot be derived from the results of this chapter.

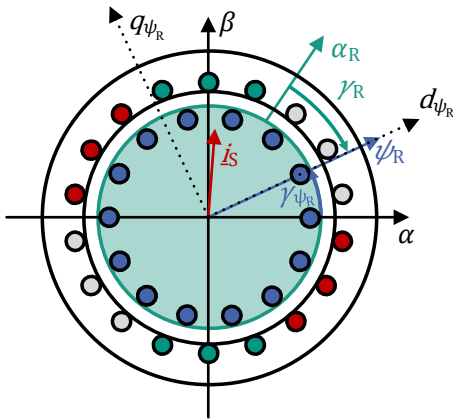


Fig. 1.: Drawing of an induction motor including all angle definitions.

The analyzed 3-phase machine is shown in fig. 1. It features one pole pair, $Q_R = 14$ rotor bars and 18 slots. The rotor is not skewed which favors the formation of harmonics [4], [14]. The flux linkage maps were generated in rotor current orientation, which differs from the rotor flux orientation used for machine control. Therefore, all maps of [4] were initially reoriented to align with rotor flux reference frame given by d_{ψ_R}, q_{ψ_R} in fig. 1. The angle γ_{ψ_R} in fig. 1 represents the transformation angle between the stator-fixed $\alpha\beta$ -reference frame and the d_{ψ_R}, q_{ψ_R} -frame in rotor flux orientation. γ_R indicates the angle between the rotor and the d_{ψ_R}, q_{ψ_R} -reference frame. Under no-load conditions, this angle is always zero as no slip is present.

The results show two dominant impacts on the harmonic flux linkage maps. One is the position of the rotor in relation to the stator and the other is the orientation of the rotor flux vector. To illustrate this, the flux linkages are analyzed for two operating points. In fig. 2, only the rotor angle γ_R is varied, while the rotor

flux angle is chosen to $\gamma_{\psi_R} = 0^\circ$. The stator current vector is chosen constant to $i_{sd} = 20$ A and $i_{sq} = -10$ A. Analyzing the results of fig. 2, γ_R shows a periodicity of $360^\circ/Q_R = 25.7^\circ$. This is to be expected, as shifting the rotor by one rotor bar division results in the same magnetic circuit and therefore the same flux linkages.

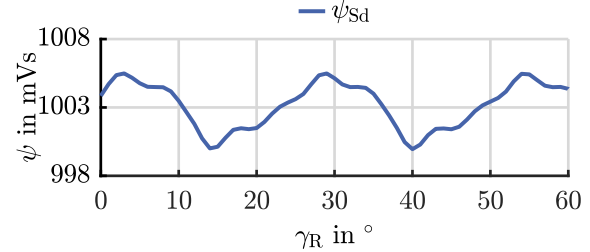


Fig. 2.: d-flux harmonics in dependence of γ_R -axis.

In fig. 3, only the rotor flux angle γ_{ψ_R} is varied, while the rotor angle is constant at $\gamma_R = 0^\circ$. The stator current vector is again chosen to $i_{sd} = 20$ A and $i_{sq} = -10$ A. This is similar to no load operation with zero slip. For γ_{ψ_R} the periodicity of the flux linkage is 60° in the RFO reference frame, which is typical for three-phase machines. It contains the dominant harmonics of the order $(6 \cdot n \pm 1)$ for $n \in \mathbb{N}^+$ in stator orientation which turn into the multiples of the 6th order through the transformation in RFO.

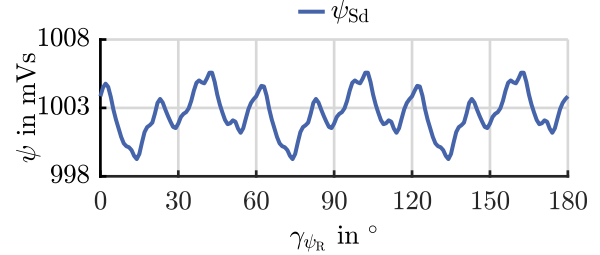


Fig. 3.: d-flux harmonics in dependence of γ_{ψ_R} -axis.

The induction motor only produces torque if the slip is not equal to zero. As a result, both angles usually vary during operation, meaning that a controller must be able to handle every possible combination of both angles. Fig. 3 shows the full harmonic flux map for the variation of both, rotor angle γ_R and rotor flux angle γ_{ψ_R} .

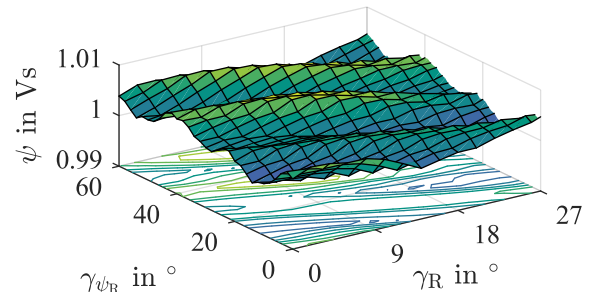


Fig. 4.: ψ_d harmonic map in dependence of γ_R -axis and γ_{ψ_R} -axis.

III. DESIGN OF THE CONTROLLER

The block diagram of the whole drive system is shown in fig. 6. The control architecture is based on the FOC published in [15]. The d- and q-axes each feature its own independent repetitive PI-controller. The block diagram of the proposed repetitive PI-controller is shown in fig. 7.

In contrast to synchronous machines, the transformation angle for the FOC for induction motors cannot be determined directly by the encoder. To ensure accurate estimation of the rotor flux angle, the non-linear current model from [16] is used. It models the non-linearity of the mutual flux as well as the change in the rotor time constant across the operating range.

A. Controller parameters

The d- and q-current path each feature its own independent repetitive PI controller, as shown in Figure 6. The controller parameters K_p and K_i for the repetitive PI controller are chosen in accordance with the modulus optimum using the datasheet values, with T_A being the controller and PWM interval.

$$K_p = \frac{L_{S,\sigma} + L_{R,\sigma}}{4 \cdot T_A} \quad (5)$$

$$K_i = \frac{R_S}{4 \cdot T_A} \quad (6)$$

B. Feedforward control

To improve dynamics, the data from the nonlinear current model and the stator current setpoint values i_{sd}^* , i_{sq}^* are used for feedforward control.

$$v_d^\Sigma = -\omega_s (L_{S,\sigma} + L_{R,\sigma}) \cdot i_{sq}^* \quad (7)$$

$$v_q^\Sigma = \omega_s \left((L_{S,\sigma} + L_{R,\sigma}) \cdot i_{sd}^* - i_\mu \cdot L_{R,\sigma} + \psi_{Rd} \right) \quad (8)$$

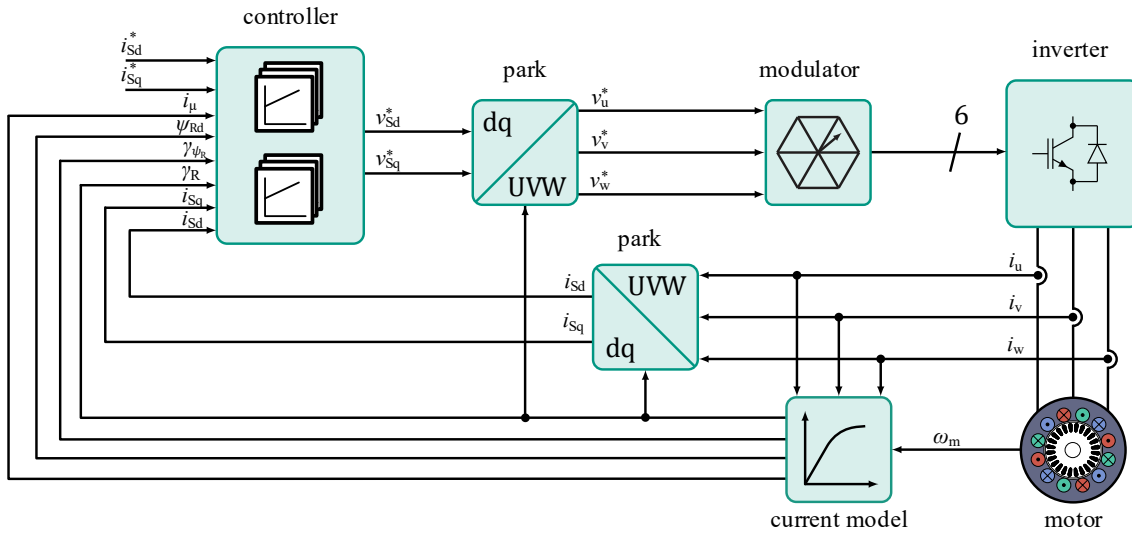


Fig. 6.: Block diagram of the drive system.

i_μ thereby denotes as the magnetization current that flows through the mutual inductance. It is further assumed that the stator and rotor leakage inductances ($L_{S,\sigma}$, $L_{R,\sigma}$) are constant across the entire operating range. They are chosen according to the datasheet values.

C. Repetitive integral path

For synchronous machines, a 1D storage system suffices because the rotor angle is used as the transformation angle for the FOC. This results only in a 1D periodicity. As discussed in Chapter II, this is not the case for induction machines. Therefore, a 2D storage system is proposed to cover both angles. Therefore, the 1D storage system known from synchronous machines is extended by the rotor angle dimension γ_R . This also allows reduction of rotor position-dependent harmonics. The procedures given in this section are identical for each repetitive controller in the d- and q-axis.

1) Interpolation and storage

The memory of the integral component can only store discrete sampling points. Therefore, the storage is based on bilinear interpolation. As the memory is 2D, all four sampling points around the measured coordinate point given by $[\gamma_R, \gamma_{\psi_R}]$ must be stored accordingly.

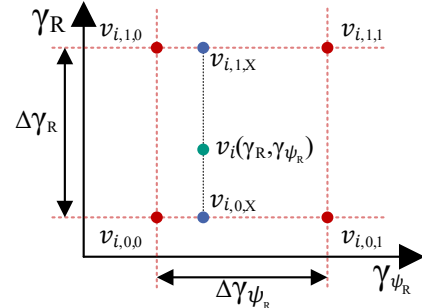


Fig. 5.: Bilinear and inverse bilinear interpolation with key variables.

Fig. 5 illustrates the basic process. For the sake of simplicity, this procedure is only shown the point $v_{i,0,0}$. The other three points are calculated similarly.

$$k_{\gamma\psi_R} = \frac{\gamma_{\psi_R} - \gamma_{\psi_R,low}}{\Delta\gamma_{\psi_R}} \quad (9)$$

$$k_{\gamma_R} = \frac{\gamma_R - \gamma_{R,low}}{\Delta\gamma_R} \quad (10)$$

$$v_{i,0,0}(t) = v_i(t-1) + \Delta i \cdot K_i \cdot T_A \cdot (1 - k_{\gamma_R})(1 - k_{\gamma\psi_R}) \quad (11)$$

The variable t thereby represents the current point in time in the time-discrete system. $(t-1)$ does not necessarily refer to the previous time step, but rather the last point in time at which the memory of that specific sampling point was updated.

For the output interpolation all 4 sampling points are necessary to calculate the output voltage $v_{i,out}$ of the integral part. The subscript '1' thereby indicates that the sampling point is larger than the desired value on the respective axes. The bilinear interpolation for the output is performed in two steps. First interpolation on the γ_R -axis is performed, resulting in two auxiliary support points on the $\gamma\psi_R$ -axis as shown in fig. 5.

$$v_{i,0,X} = v_{i,0,0} \cdot (1 - k_{\gamma_R}) + v_{i,0,1} \cdot k_{\gamma_R} \quad (12)$$

$$v_{i,1,X} = v_{i,1,0} \cdot (1 - k_{\gamma_R}) + v_{i,1,1} \cdot k_{\gamma_R} \quad (13)$$

The output voltage of the integral part is subsequently calculated by linear interpolation between the auxiliary support points.

$$v_{i,out} = v_{i,1,0} \cdot (1 - k_{\gamma\psi_R}) + v_{i,1,1} \cdot k_{\gamma\psi_R} \quad (14)$$

2) Symmetries

As the controller's transient performance decreases by the number of grid points in the integral path, the storage size of the 2D controller is reduced utilizing the symmetries shown in chapter II. It covers only one period of $\gamma\psi_R$ being $[0^\circ, 60^\circ]$ and γ_R being $[0^\circ, 360/Q_R^\circ]$.

The use of symmetries is thereby always a trade-off between settling time and remaining current ripple as further harmonics can occur in the real machine due to the design, production, ageing, faults etc. Furthermore, the power converter adds nonlinearities to the system.

As these effects may not follow the same periodicity as the ideal symmetrical machine, compensation using this repetitive control approach can only be achieved for full periods of each signal. Therefore, the range would typically be chosen to full mechanical periods of the rotor and stator. This would lead to long settling times and huge storage sizes. Consequently, only the repetitive control approach utilizing the symmetries was implemented.

3) Choosing the size of the lookup tables

According to the sampling theorem, higher frequency components can be reconstructed if the sampling frequency is increased. This means that higher harmonic orders can be compensated by the repetitive control if the angular resolution is high. For this reason, it would be desirable to implement the highest possible number of support points in a system to achieve the lowest possible current ripple.

There are some limitations that must be taken into account when determining the number of support points:

1. The settling time of the repetitive control increases with the total number of support points of each controller. Meaning that changing a system from a PI to a 2D repetitive PI controller with a lookup table of the size of $n_{\gamma_R} = 4$ and $n_{\gamma\psi_R} = 4$ can increase the settling time up to a factor of 16.
2. The controller should update each of the support points consecutively within a full period to avoid disturbances. Hence, that the number of support points may need to be decreased when the angular velocity in either of the axes increases.

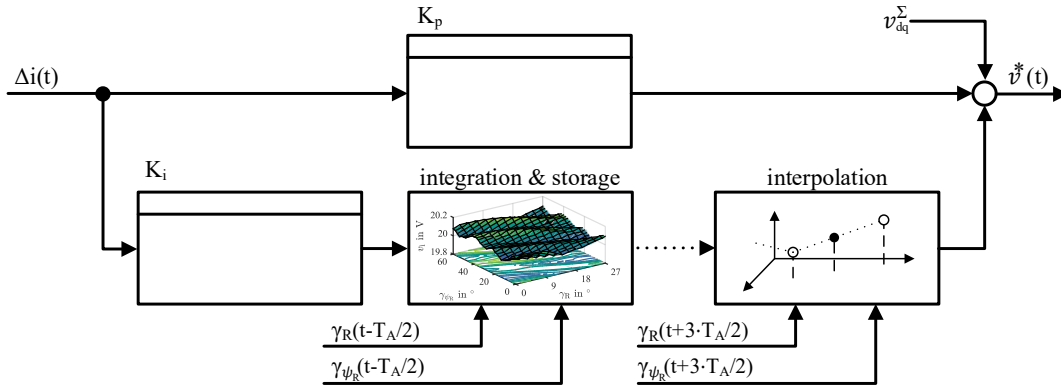


Fig. 7.: Simplified block diagram of the proposed 2D repetitive PI Control.

IV. TESTBENCH SETUP

The test setup consists of a signal processing system and power electronics, which were specifically developed for research purposes [17], [18]. The DUT and load machine used are commercially available machines from Siemens with their characteristics given in section B.

A. Power Converters and Signal Processing

The signal processing system of the testbench based on a Xilinx Zynq 7030 [18]. To allow a fast adaptation of the software to different test scenarios, the programming is performed using *MATLAB® Simulink Code generation*. The rotor angle is measured by a 10-bit incremental encoder, which is operated with 4-fold evaluation, resulting in absolute angular resolution of 12-bit.

The test bench runs at a switching and controller frequency of 10 kHz. The DUT and load machine are powered by the two-level IGBT *ETI-EPSR* shown in [17]. It features *LEM LA 100-P* sensors for current measurement with an accuracy of 0.5 %. The signals are recorded by a *Texas Instruments THS1206* 12-bit AD converter with 1.5 MSPS per channel and averaged for each switching period.

B. Device under test

The testbench is shown in fig. 8. It has two *Siemens 1LE1592-1EB42-1AF4* SCIM as DUT and load. Both feature a sensor for stator temperature monitoring. Rotor temperature sensing is not provided.

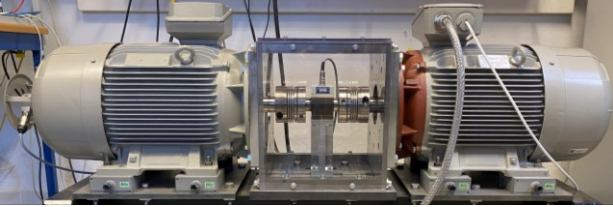


Fig. 8.: Testbench of the *Siemens 1LE1592-1EB42-1AF4*.

The basic machine data according to the datasheet is given in Table I [19]. It is used for parameterization of the proposed repetitive PI control. The load machine is speed controlled by a cascaded PI control using the same datasheet values. Fig. 9 shows the d-flux linkage of the DUT as published in [16].

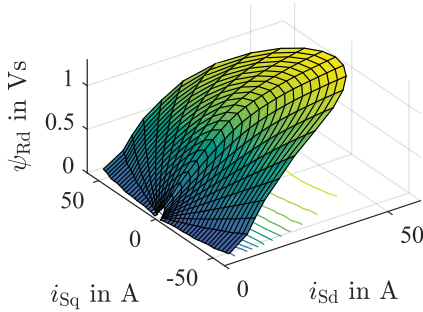


Fig. 9.: Rotor flux linkage in rotor flux orientation [16].

The d-flux linkage shows significant saturation, particularly at d-currents above 20 A. It is assumed that the leakage flux is approximately linear and thus the leakage inductances are not significantly affected by saturation. As the controller parameters are chosen in relation to the leakage inductances stable control over the entire operating range is possible.

The feed-forward control based on the nonlinear current model uses the identified flux linkage maps of [16] to calculate the rotor flux. This improves the overall performance of the system but is not generally necessary for operation. To enable precise determination of the rotor flux angle γ_{ψ_R} , the nonlinear current model utilizes the measured rotor time constant maps as shown in Fig. 9.

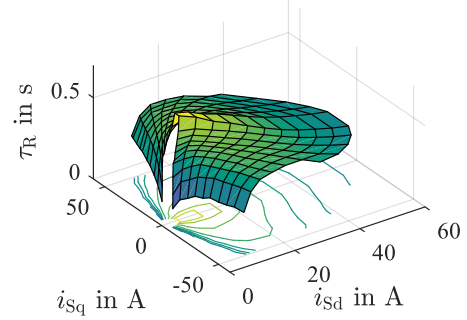


Fig. 9.: Measured rotor time constant based on transient measurements [16].

Since the internal design of the DUT is not known, the periodicity of the rotor had to be determined by additional measurements. For this purpose, the dominant harmonics of the rotor were identified in a voltage-controlled operation using 2D FFTs of the currents. The 14th harmonic was identified as the first dominant order for the rotor angle axis resulting in the same periodicities as the FEA results shown in chapter II.

TABLE I. LINEAR CHARACTERISTICS OF THE DUT [19]

Symbol	Meaning	Value
P_N	Nominal power	22 kW
I_N	Nominal current	45 A
n_N	Nominal speed	1500 rpm
p	Pole pairs	2
R_S	Stator resistance	154 mΩ
R_R	Rotor resistance	103 mΩ
$L_{S\sigma}$	Stator leakage inductance	2.5 mH
$L_{R\sigma}$	Rotor leakage inductance	0.93 mH

V. MEASUREMENT RESULTS

All measurements were performed with the setup described in section IV at 750 rpm and 10 kHz switching and controller frequency.

Due to the symmetries of the used machine, the angular range of the 2D repetitive controllers was chosen to 25.7° for γ_R and 60° for γ_{ψ_R} . The number of grid points on the γ_R -axis is 6, for the γ_{ψ_R} -axis 14. According to the sampling theorem compensation up to the 42nd harmonic both axes is theoretically possible.

For comparison, measurements were also carried out with a PI control and a 1D repetitive control with identical controller parameters. Along the γ_{ψ_R} -axis, the number of grid points for the 1D repetitive control was set to 48 for an angular range of 180° . According to the sampling theorem, compensation up to the 48th order is therefore theoretically possible. Due to the 1D approach, no compensation along the γ_R -axis is possible.

A. No-load operation

Fig. 11 shows the amplitude spectrum of the measured stator currents $|F_{ids}|$ and $|F_{iqs}|$ for the different controllers. The operating point is chosen to $i_{sd} = 20$ A and $i_{sq} = 0$ A at 750 rpm. At this operating point, the rotor frequency is zero, as no load is present.

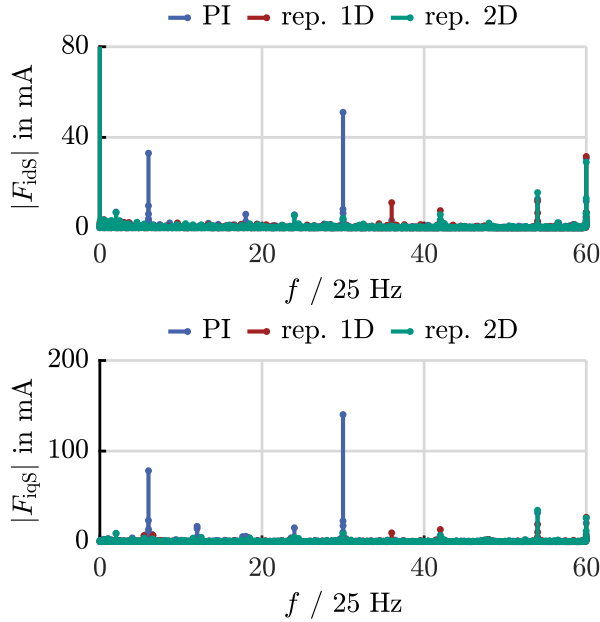


Fig. 11.: Harmonic content of the stator currents at $i_{sd} = 20$ A and $i_{sq} = 0$ A of a 1D and 2D repetitive PI control compared to a conventional PI control.

The spectrum clearly demonstrates the superior performance of both repetitive control algorithms compared to the conventional PI control. The stator harmonics, which are periodic to the γ_{ψ_R} -axis can be filtered effectively by both repetitive controllers. This is also reflected in total harmonic distortion of the d-current. It improves for both repetitive control algorithms by $\Delta\text{THD}_\% = 1.1\%$. Due to the increased angular

range of the 1D repetitive control, slightly better performance for low frequency harmonics can be observed.

As the rotor angle almost constant during operation, only slight rotor harmonics are visible, which can be compensated by the 2D controller. Overall, the 2D approach has no big advantage over the 1D approach in this operating point. Above the 42nd and 48th harmonic no further damping of the current harmonics is possible by the repetitive controllers, which is also reflected in the spectrum.

B. On-load operation

The operating point for the on-load operation is chosen to $i_{sd} = i_{sq} = 15$ A. As this operating point produces torque, slip is present and the rotor frequency is greater than zero.

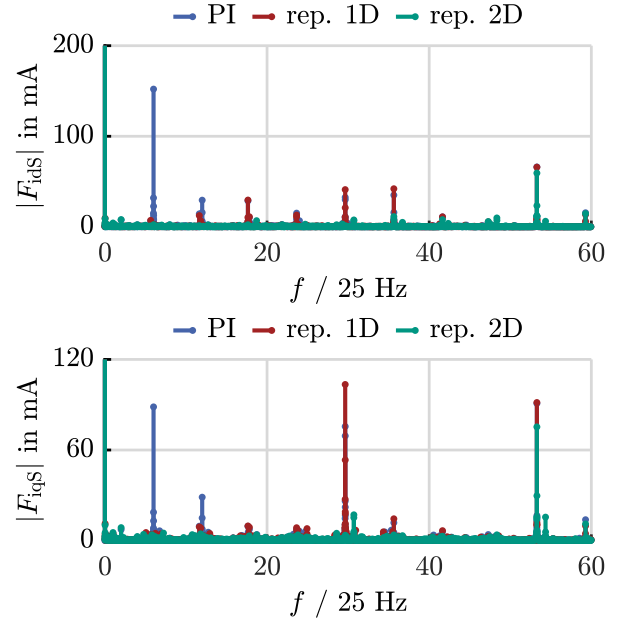


Fig. 12.: Harmonic content of the stator currents at $i_{sd} = i_{sq} = 15$ A of a 1D and 2D repetitive PI control compared to a conventional PI control.

Fig. 12 shows the amplitude spectrum of the measured stator currents $|F_{ids}|$ and $|F_{iqs}|$ for the different controllers. Again, the spectrum shows a clear improvement for the repetitive controllers. This is also evident in THD values given in Table II.

TABLE II. TOTAL HARMONIC DISTORTION AT ON LOAD OPERATION

Control Typ	$\text{THD}_\% - i_{sd}$	$\text{THD}_\% - i_{sq}$
PI control	12.4 %	11.9 %
1D repetitive PI control	7.1 %	10.7 %
2D repetitive PI control	5.4 %	6.7 %

In contrast to the no-load operation, the THD values further improve if a second dimension is added to the repetitive controller. This is due to the rotor angle γ_R not being constant for this operating point and the harmonics caused by the rotor angle dependency are not periodic to the γ_{ψ_R} -axis. Therefore, damping is not possible for the 1D controller.

By adding the second dimension, the 2D repetitive control can further reduce the harmonic content of the γ_R -axis, making it a suitable solution for induction machines. As the rotor harmonics are usually small compared to the stator harmonics, a significant improvement in THD is possible even with the 1D repetitive control. The spectrum also shows, that above the 42nd and 48th harmonic no further damping of the current harmonics is possible by the repetitive controllers. By increasing the switching and controller frequency or lowering the rotational speed, higher harmonic orders could be compensated as well.

VI. CONCLUSION

This paper presents a novel 2D repetitive control technique. The efficient and powerful design of the controller makes it easy to use in various areas such as parameter identification and reduction of torque harmonics. In addition, it can improve the efficiency by eliminating the harmonic current components. The superior performance of the presented controller has been confirmed by testbench measurements and compared with a conventional PI control and a 1D repetitive PI control.

The fundamental disadvantage of this approach is the increased settling time. This effect is aggravated by the low rotor frequency in the 2D approach. It was partly mitigated by utilizing the machine symmetries. Nevertheless, the dynamics of a simple PI controller can generally not be achieved with the repetitive PI control approach.

VII. REFERENCES

- [1] Y. Wang, J. Yang, G. Yang, S. Li, and R. Deng, "Harmonic currents injection strategy with optimal air gap flux distribution for multiphase induction machine," *IEEE Trans. Power Electron.*, vol. 36, no. 1, pp. 1054–1064, Jan. 2021, doi: 10.1109/TPEL.2020.3001124.
- [2] C. Debruyne, J. Desmet, S. Derammelaere, and L. Vandevelde, "Derating factors for direct online induction machines when supplied with voltage harmonics: A critical view," in *2011 IEEE International Electric Machines & Drives Conference (IEMDC)*, Niagara Falls, ON, Canada: IEEE, May 2011, pp. 1048–1052. doi: 10.1109/IEMDC.2011.5994745.
- [3] S. Khomfoi, V. Kinnares, and P. Viriya, "Influence of PWM characteristics on the core losses due to harmonic voltages in PWM fed induction motors," in *2000 IEEE Power Engineering Society Winter Meeting. Conference Proceedings (Cat. No.00CH37077)*, Singapore: IEEE, 2000, pp. 365–369. doi: 10.1109/PESW.2000.849991.
- [4] J. Stoss, P. Mader, L. Geier, A. Karayel, A. Liske, and M. Hiller, "Efficient nonlinear modelling of spatial flux harmonics of squirrel cage induction motors using inverse flux maps and static FEA," in *2024 IEEE 10th International Power Electronics and Motion Control Conference (IPEMC2024-ECCE Asia)*, May 2024. doi: 10.1109/IPEMC-ECCEAsia60879.2024.10567693.
- [5] V. Kindl, R. Cermak, Z. Ferkova, and B. Skala, "Review of Time and Space Harmonics in Multi-Phase Induction Machine," *Energies*, vol. 13, no. 2, p. 496, Jan. 2020, doi: 10.3390/en13020496.
- [6] A. Mollaecian, S. M. Sangdehi, A. Balamurali, G. Feng, J. Tjong, and N. C. Kar, "Reduction of space harmonics in induction machines incorporating rotor bar optimization through a coupled IPSO and 3-D FEA algorithm," in *2016 XXII International Conference on Electrical Machines (ICEM)*, Lausanne, Switzerland: IEEE, Sep. 2016, pp. 557–563. doi: 10.1109/ICELMACH.2016.7732581.
- [7] J. Richter, T. Lannert, T. Gemassmer, and M. Doppelbauer, "Mitigation of Current Harmonics in Inverter-Fed Permanent Magnet Synchronous Machines with Nonlinear Magnetics," *Proc. PCIM Eur. 2015 Int. Exhib. Conf. Power Electron. Intell. Motion Renew. Energy Energy Manag.*, pp. 1–8, 2015, doi: 10.5445/IR/1000048319.
- [8] A. R. Munoz and T. A. Lipo, "On-line dead-time compensation technique for open-loop PWM-VSI drives," *IEEE Trans. Power Electron.*, vol. 14, no. 4, pp. 683–689, Jul. 1999, doi: 10.1109/63.774205.
- [9] F. Xie, K. Liang, W. Wu, W. Hong, and C. Qiu, "Multiple Harmonic Suppression Method for Induction Motor Based on Hybrid Morphological Filters," *IEEE Access*, vol. 7, pp. 151618–151627, Jan. 2019, doi: 10.1109/ACCESS.2019.2948276.
- [10] C. Sheng, Q. Wang, T. Su, and H. Wang, "Induction motor torque closed-loop vector control system based on flux observation and harmonic current suppression," *Control Eng. Pract.*, vol. 142, p. 105755, Jan. 2024, doi: 10.1016/j.conengprac.2023.105755.
- [11] K. Yu, W. Xu, Y. Liu, and J. Gao, "Harmonics Mitigation of Standalone Brushless Doubly-Fed Induction Generator Feeding Nonlinear Loads Considering Power Converter Voltage Rating," in *2018 IEEE Energy Conversion Congress and Exposition (ECCE)*, Portland, OR, USA: IEEE, Sep. 2018, pp. 6989–6995. doi: 10.1109/ECCE.2018.8557704.
- [12] C. Liu, F. Blaabjerg, W. Chen, and D. Xu, "Stator Current Harmonic Control With Resonant Controller for Doubly Fed Induction Generator," *IEEE Trans. Power Electron.*, vol. 27, no. 7, pp. 3207–3220, Jan. 2012, doi: 10.1109/TPEL.2011.2179561.
- [13] S. Haehnlein, J. P. Degel, C. Kloeffer, and M. Doppelbauer, "Current Harmonics Control Algorithm for inverter-fed Nonlinear Synchronous Electrical Machines," in *2023 IEEE International Electric Machines & Drives Conference (IEMDC)*, San Francisco, CA, USA: IEEE, May 2023, pp. 1–6. doi: 10.1109/IEMDC55163.2023.10238964.
- [14] T. Gundogdu, Z. Q. Zhu, J. C. Mipo, and S. Personnaz, "Influence of Rotor Skew on Rotor Bar Current Waveform and Performance in Induction Machines," in *2018 21st International Conference on Electrical Machines and Systems (ICEMS)*, Jeju: IEEE, Oct. 2018, pp. 525–530. doi: 10.23919/ICEMS.2018.8549245.
- [15] F. Blaschke, "Das Verfahren der Feldorientierung zur Regelung der Drehfeldmaschine," 1973.

- [16] J. Stoß, A. Karayel, L. Geier, A. Liske, and M. Hiller, "Identification of rotor and stator flux linkage maps of squirrel cage induction motors based on identification of rotor time constant maps," in *2023 25th European Conference on Power Electronics and Applications (EPE'23 ECCE Europe)*, Aalborg, Denmark: IEEE, Sep. 2023, pp. 1–11. doi: 10.23919/EPE23ECCEurope58414.2023.10264589.
- [17] Rüdiger Schwendemann, Simon Decker, Marc Hiller, and Michael Braun, "Modular Converter- and Signal-Processing-Platform for Academic Research in the Field of Power Electronics," IEEE, Karlsruhe, Germany, 2016.
- [18] B. Schmitz-Rode *et al.*, "A modular signal processing platform for grid and motor control, HIL and PHIL applications," in *2022 International Power Electronics Conference (IPEC-Himeji 2022- ECCE Asia)*, Himeji, Japan: IEEE, May 2022, pp. 1817–1824. doi: 10.23919/IPEC-Himeji2022-ECCE53331.2022.9807061.
- [19] Siemens AG, "Datasheet: Siemens 1LE1592-1EB42-1AF4." [Online]. Available: <https://mall.industry.siemens.com/mall/de/DE/Catalog/Product/teddatasheet/?format=PDF&caller=Mall&mlfbs=1LE1592-1EB42-1AF4%20%20&language=de>